

Article

Robust Online Estimation of State of Health for Lithium-Ion Batteries Based on Capacities under Dynamical Operation Conditions

Xiaoxuan Wu ¹, Jian Chen ^{2,*}, Hu Tang ¹, Ke Xu ³, Mingding Shao ^{2,3} and Yu Long ^{1,4,*}

¹ State Key Laboratory of Featured Metal Materials and Life-Cycle Safety for Composite Structures, Guangxi University, Nanning 530004, China; wuxiaoxuan@st.gxu.edu.cn (X.W.); abc123@st.gxu.edu.cn (H.T.)

² State Key Laboratory of Fluid Power and Mechatronic Systems, School of Mechanical Engineering, Zhejiang University, Hangzhou 310027, China; 22160703@zju.edu.cn

³ Department of System Engineering, Wanxiang A123 Systems Corp., Hangzhou 311215, China; kexu@a123systems.com

⁴ Institute of Data Science and Intelligent Systems, Northwestern Polytechnical University, Xi'an 710072, China

* Correspondence: jchen@zju.edu.cn (J.C.); longyu@gxu.edu.cn (Y.L.).

Abstract: Lithium-ion batteries, as the main energy storage component of electric vehicles (EVs), play a crucial role in ensuring the safe and reliable operation of the battery systems through monitoring their state of health (SOH). However, temperature variations and battery aging have significant impacts on the internal parameters of lithium-ion batteries, and these changes directly correlate with the accuracy of battery SOH estimation. To address these issues, this paper proposes an estimation method for lithium-ion battery SOH that considers the impact of temperature. The method begins with reconstructing a second-order hybrid equivalent circuit model for lithium-ion batteries, through which an adaptive update rate for battery model parameters is designed. On this basis, a nonlinear observer for battery states is introduced by integrating filters to estimate SOH. The proposed method considers the impact of capacity in the design of the parameter adaptive update rate, enabling the capacity to be dynamically adjusted based on the actual state of the batteries. This reduces the cumulative error in the SOC observer and improves the modeling accuracy of battery models. Experimental results demonstrate that the method proposed in this paper exhibits exceptional performance in SOH estimation under different temperature conditions. The mean absolute error for SOH estimation does not exceed 0.5%, and the root mean square error does not exceed 0.2%. This method can significantly improve the estimation accuracy of SOH, providing a more efficient and accurate solution for battery management systems in EVs.

Keywords: lithium-ion battery; state of health; state of charge; parameter estimation



Citation: Wu, X.; Chen, J.; Tang, H.; Xu, K.; Shao, M.; Long, Y. Robust Online Estimation of State of Health for Lithium-Ion Batteries Based on Capacities under Dynamical Operation Conditions. *Batteries* **2024**, *10*, 219. <https://doi.org/10.3390/batteries10070219>

Academic Editor: Ottorino Veneri

Received: 20 May 2024

Revised: 7 June 2024

Accepted: 13 June 2024

Published: 22 June 2024



Copyright: © 2024 by the authors. Licensee MDPI, Basel, Switzerland. This article is an open access article distributed under the terms and conditions of the Creative Commons Attribution (CC BY) license (<https://creativecommons.org/licenses/by/4.0/>).

1. Introduction

Lithium-ion batteries, as an indispensable energy storage component in electric vehicles (EVs), have a direct impact on the overall performance of products [1]. With the widespread application of lithium-ion batteries, the issue of battery aging has gradually become prominent. Battery aging not only leads to a decrease in battery capacity and an increase in internal resistance, but also may trigger safety issues such as thermal runaway [2]. The state of health (SOH) of lithium-ion batteries describes the current degree of battery aging, which is of great significance for the safe use, performance optimization, and life extension of batteries [3]. Therefore, accurately estimating the SOH of batteries is crucial for ensuring the safe and reliable operation of battery systems. Generally, SOH is defined as the ratio of the current battery capacity to the new battery capacity, but this requires knowing the initial capacity of the battery [4], which is often difficult to accurately obtain in practice. The aging process of batteries has nonlinear characteristics, meaning that the rate of battery

capacity decay is not constant but varies with time and usage conditions. This makes it difficult for traditional linear estimation methods to accurately describe the battery aging process. Moreover, the complex electrochemical processes inside lithium-ion batteries and external environmental factors make the precise estimation of SOH a challenging issue [5].

Estimation methods for SOH range from experimental estimation techniques to model-based approaches. Experimental estimation techniques evaluate battery degradation states through laboratory tests such as capacity testing [6], internal resistance testing [7], electrochemical impedance spectroscopy (EIS) [8], charge curve analysis [9], ultrasonic analysis [10], incremental capacity analysis (ICA) [11], and differential voltage analysis (DVA) [12]. Although experimental estimation techniques can provide rich degradation information and accurate SOH estimation results, practical applications prefer online, real-time, and reliable SOH monitoring. Model-based estimation methods, especially data-driven algorithms and adaptive filtering techniques, provide effective solutions for this demand [13]. Data-driven techniques utilize machine learning algorithms and vast amounts of historical data to train models, thereby predicting the SOH of batteries. Optimization algorithms [14], empirical and fitting techniques [15], sample entropy techniques [16], and machine learning techniques [17] are typical representatives of data-driven methods. Among them, support vector machines (SVMs) [18], neural networks (NNs) [19], physics-informed neural networks (PINNs) [20], and fuzzy logic (FL) [21] can automatically learn patterns of battery aging from large amounts of data and make SOH predictions accordingly. These methods can handle complex battery dynamics and uncertain operating environments, but they usually require significant training data and computational resources, which may be limited in real-time applications.

Adaptive filtering or observer methods estimate the SOH by establishing physical or statistical models of batteries and combining real-time measured current and voltage data. This approach is better at capturing changes in the battery system's state, demonstrating excellent performance in dynamic adjustment and real-time response. Among them, electrochemical models (EMs) provide in-depth understanding and accurate predictions of battery behavior based on the chemical reaction kinetics within the battery, but they are characterized by complex modeling and high computational costs [22]. In contrast, equivalent circuit models (ECMs) describe batteries through simplified circuit elements, offering advantages such as a simple structure and fast solution speed, making them the most widely used models [23]. Kalman filtering and its derivative algorithms, such as the extended Kalman filter (EKF) [24], the unscented Kalman filter (UKF) [25], and the particle filter (PF) [26], provide powerful tools for handling battery's nonlinear dynamic characteristics and uncertainties. Plett [27] introduced a dual extended Kalman filter (DEKF) to simultaneously update battery SOC estimation and capacity. Considering the inconsistency between the rapid changes in SOC and the gradual changes in battery capacity, a multi-timescale DEKF was designed by separating the time scales of the state estimation filter and the parameter estimation filter [28]. Since EKF may perform poorly in highly nonlinear systems, Xiong et al. [29] proposed a DUKF method to enhance the estimation accuracy of SOC and parameters.

It is worth noting that a battery's SOH directly impacts its available energy and charging capacity, thereby further influencing its state of charge (SOC). Therefore, there exists a circular dependency between these two states. In addition, battery model parameters are influenced by multiple factors such as battery type, operating temperature, cycling history, and SOC. Ignoring the time-varying parameters in the battery model can lead to a decrease in modeling accuracy, which subsequently affects estimation precision. SOH estimation, considering the changes in battery model parameters, can more accurately assess the overall performance and remaining lifespan of the battery. Yu et al. [30] proposed an online capacity estimation method based on the recursive least squares and adaptive H_∞ filter (RLS-AHIF) joint estimation filter. A RLS algorithm was used to realize the online parameter identification of the battery model, and then an adaptive H_∞ filter was used to estimate the SOH of the battery. To address the issue of RLS's insensitivity to sudden

changes in battery states, the forgetting factor recursive least squares (FFRLS) method was employed to update model parameters in real time [31]. The total least squares (TLS) method was adopted to estimate battery capacitance, improving the prior estimation accuracy of SOC. Finally, the UKF was utilized to estimate the precision of SOC, resulting in a more accurate SOH estimation. Nonlinear observers have also been applied for SOH estimation. Zhou et al. [32] proposed a cascaded fractional-order sliding mode observer (FOSMO) for estimating the SOC and SOH of lithium-ion batteries. They utilized the terminal voltage, polarization voltage, and open-circuit voltage to estimate the SOC. Moreover, two FOSMOs were developed to estimate the capacity and internal resistance of lithium-ion batteries for estimating the SOH.

Current model-based SOH estimation frameworks separate the design of battery model parameter identification and state estimation. The parameters of the model are updated in real time by the least squares method or sliding mode observer, and then the existing state estimation method is introduced to estimate the SOH. These approaches require multiple transformations of the battery model, introducing a certain level of complexity. To address these issues, we refer to the observer design of [33] and propose a joint SOC and SOH estimation method that can realize both parameter identification and state estimation [34]. However, this method sets the battery capacity to a fixed value, resulting in a small cumulative error in the SOC observer.

Considering that capacity is also included in the parameter adaptive update rate design, a filter-based SOH estimation method for lithium-ion batteries is proposed. Firstly, the chosen second-order mixed equivalent circuit model for lithium-ion batteries was reconstructed, transforming the expression of terminal voltage derivative into the product of measurable variables, non-measurable variables, and an unknown parameter matrix. This unknown parameter matrix encompasses all time-varying parameters of the battery model, and a parameter adaptive update rate was designed to achieve online updates of the battery model. Subsequently, a cascaded estimator for SOC, short-term and long-term transient response voltages of the battery, and the terminal voltage were designed to realize SOH estimation. Traditional methods lack experimental validation and comparison under different temperatures and operating conditions. We designed lithium-ion battery experiments at different temperatures and compared them with the DEKF and DUKF methods. The experimental results show that the proposed method exhibits better performance and effectiveness under various operating conditions. The main contributions of this paper are as follows: (1) The proposed method improves the accuracy and real-time performance of SOH estimation through the online updating of the battery model. (2) The multi-cascade design can more accurately capture changes in the battery status, improving the accuracy of SOH estimation. (3) By considering the dynamic changes in capacity, the cumulative error in the SOC observer is reduced, and the battery model modeling accuracy is improved.

The following parts of this paper are organized as follows: Section 2 describes the second-order hybrid equivalent circuit model of lithium-ion battery and the proposed reconstruction method of the battery model. Section 3 describes the filter-based estimation method of SOH and the adaptive update rate design of battery model parameters. The stability analysis of the algorithm is shown in Section 4. Section 5 introduces the experimental platform and analyzes the experimental results. Finally, Section 6 summarizes the conclusions of this paper.

2. Mathematical Modeling of Lithium-Ion Batteries

A second-order hybrid equivalent circuit model of a lithium-ion battery was employed to simulate the battery's structure [35,36], as depicted in Figure 1. In contrast to conventional equivalent models, it possesses the capability to precisely anticipate both the steady state and transient response behaviors of the battery by leveraging its distinctive array of components and interdependencies. This model comprehensively encapsulates the dynamic circuit attributes of the battery, encompassing the open circuit voltage, terminal voltage, transient response, and self-discharge phenomena.

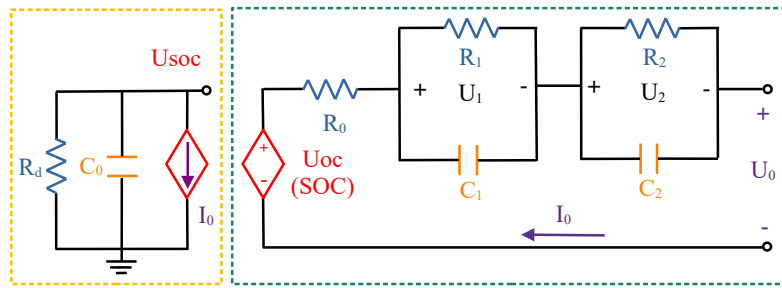


Figure 1. Second-order hybrid equivalent circuit model for lithium-ion batteries (The orange box indicates the SOC characteristics of the lithium-ion battery, and the green box indicates the transient response characteristics of the voltage and current of the lithium-ion battery).

The subcircuits on the left side of Figure 1 represent lithium-ion battery SOC tracking and the runtime prediction. A self-discharge resistor R_d is used to characterize the self-discharge energy loss of the battery. The current control current source I_0 charges and discharges C_0 are used to characterize the total amount of electricity stored in the battery, so that the dynamic change of $SOC \in [0\%, 100\%]$ is represented by $U_{SOC} \in [0 \text{ V}, 1 \text{ V}]$. Thus, the U_{SOC} expression is given by

$$\dot{U}_{SOC} = -\frac{\eta_0}{R_d C_0} U_{SOC} - \frac{\eta_0}{C_0} I_0 \quad (1)$$

where η_0 is the Cullen efficiency. The subcircuit on the right side of Figure 1 represents the transient response characteristics of the voltage and current. The voltage source $U_{OC}(U_{SOC})$ is applied to connect the open-circuit voltage U_{OC} to the SOC of the battery, and the nonlinear relationship between the open-circuit voltage U_{OC} and the SOC is expressed as $U_{OC} = \varphi(U_{SOC})$. U_0 is the terminal voltage of the battery, and R_0 is the internal resistance, which is used to characterize the energy loss of the battery in charging and discharging. R_1, C_1, R_2 , and C_2 denote the short-term and long-term transient responses of the battery, and the mathematical relationships of the short-term and long-term transient response voltages U_1 and U_2 are as follows:

$$\dot{U}_1 = -\frac{1}{R_1 C_1} U_1 + \frac{1}{C_1} I_0 \quad (2)$$

$$\dot{U}_2 = -\frac{1}{R_2 C_2} U_2 + \frac{1}{C_2} I_0. \quad (3)$$

According to Kirchhoff's voltage law, the battery terminal voltage can be written as:

$$U_0 = U_{OC} - R_0 I_0 - U_1 - U_2. \quad (4)$$

Combining the SOC characteristics and the transient response characteristics of the battery voltage and current, the derivative expression for the battery terminal voltage U_0 is given by:

$$\begin{aligned} \dot{U}_0 &= \dot{U}_{OC} - R_0 \dot{I}_0 - \dot{U}_1 - \dot{U}_2 \\ &= \dot{\varphi}(U_{SOC}) \dot{U}_{SOC} - R_0 \dot{I}_0 - \frac{U_1}{R_1 C_1} - \frac{U_2}{R_2 C_2} + \left(\frac{1}{C_1} + \frac{1}{C_2} \right) I_0. \end{aligned} \quad (5)$$

Adding or subtracting one term $\frac{U_0}{R_1C_1} + \frac{U_0}{R_2C_2}$ from Equation (5) gives:

$$\begin{aligned}\dot{U}_0 &= -\frac{U_0}{R_1C_1} - \frac{U_0}{R_2C_2} + \dot{\varphi}(U_{SOC}) \left(\frac{\eta_0}{R_dC_0} U_{SOC} - \frac{\eta_0}{C_0} I_0 \right) - R_0 \dot{I}_0 \\ &\quad - \left(-\frac{1}{R_1C_1} U_1 + \frac{1}{C_1} I_0 \right) - \left(-\frac{1}{R_2C_2} U_2 + \frac{1}{C_2} I_0 \right) + \frac{U_0}{R_1C_1} + \frac{U_0}{R_2C_2} \\ &= -\left(\frac{1}{R_1C_1} + \frac{1}{R_2C_2} \right) U_0 + \dot{\varphi}(U_{SOC}) \frac{\eta_0}{R_dC_0} U_{SOC} + \left(\frac{1}{R_1C_1} + \frac{1}{R_2C_2} \right) \dot{\varphi}(U_{SOC}) \\ &\quad - R_0 \dot{I}_0 - \frac{U_2}{R_1C_1} - \frac{U_1}{R_2C_2} - \left(\dot{\varphi}(U_{SOC}) \frac{\eta_0}{C_0} + \frac{1}{C_1} + \frac{1}{C_2} + \frac{R_0}{R_1C_1} + \frac{R_0}{R_2C_2} \right) I_0.\end{aligned}\tag{6}$$

The state variables SOC, U_1 , and U_2 within the lithium-ion battery model are inherently non-measurable, while the parameters of the battery model remain unknown and are influenced by factors such as battery SOC and temperature. Various techniques exist for identifying the parameters of the battery equivalent model, including recursive least squares (RLS) [37], genetic algorithms (GAs) [14], and particle swarm optimization (PSO) [38]. However, these methods primarily focus on enhancing modeling accuracy through adaptive battery models rather than directly estimating battery capacity. Achieving SOH estimation necessitates integrating additional algorithms into this framework. Consequently, algorithm design for parameter and state estimation mandates separate mathematical transformations of the battery model, inevitably amplifying complexity.

To facilitate the integration of parameter estimation and state estimation within the algorithmic framework, the expression for the derivative of the battery terminal voltage is reformulated as the product of the measurable variable matrix $Y \in \mathbb{R}^{1 \times 5}$, the non-measurable variable matrix $W \in \mathbb{R}^{5 \times 8}$, and the unknown parameter matrix $\theta \in \mathbb{R}^8$. Moreover, the U_{SOC} is replaced by the SOC. Unlike the battery model described in [34], which assumes a fixed battery capacity, the capacity is also included in the unknown parameter matrix. Thus, the mathematical depiction of the second-order hybrid equivalent circuit model of the lithium-ion battery illustrated in Figure 1 can be succinctly represented as:

$$\begin{cases} \dot{x}_1 = -ax_1 - bu \\ \dot{x}_2 = -\theta_1 x_2 + \theta_5 u \\ \dot{x}_3 = -\theta_2 x_3 + \theta_6 u \\ \dot{x}_4 = YW\theta \end{cases}\tag{7}$$

where $x_1 \triangleq SOC \in \mathbb{R}$, $x_2 \triangleq U_1 \in \mathbb{R}$, $x_3 \triangleq U_2 \in \mathbb{R}$, $x_4 \triangleq U_0 \in \mathbb{R}$, and $u \triangleq I_0 \in \mathbb{R}$. The matrices Y , W , and θ are expressed as

$$Y = [x_4 \quad 1 \quad 1 \quad u \quad \dot{u}]$$

$$V = \begin{bmatrix} -1 & -1 & 0 & 0 & 0 & 0 & 0 & 0 \\ \varphi(x_1) & \varphi(x_1) & -a\dot{\varphi}(x_1)x_1 & 0 & 0 & 0 & 0 & 0 \\ -x_3 & -x_2 & 0 & 0 & 0 & 0 & 0 & 0 \\ 0 & 0 & -b\dot{\varphi}(x_1) & 0 & -1 & -1 & -1 & -1 \\ 0 & 0 & 0 & -1 & 0 & 0 & 0 & 0 \end{bmatrix}$$

$$\theta = [\theta_1 \quad \theta_2 \quad \theta_3 \quad \theta_4 \quad \theta_5 \quad \theta_6 \quad \theta_7 \quad \theta_8]^T$$

with

$$a = \frac{\eta_0}{R_d}, b = \eta_0,$$

$$\theta_1 = \frac{1}{R_1C_1}, \theta_2 = \frac{1}{R_2C_2}, \theta_3 = \frac{1}{C_0}, \theta_4 = R_0,$$

$$\theta_5 = \frac{1}{C_1}, \theta_6 = \frac{1}{C_2}, \theta_7 = \frac{R_0}{R_1C_1}, \theta_8 = \frac{R_0}{R_2C_2}.$$

Remark 1. According to the analysis of Remark 1 in [34,36], it is assumed that under the stable condition of the battery system, the current and voltage of the battery are within the bounded range, so the state of the battery equivalent model is bounded, and the battery model parameters are positive and bounded. Therefore, $x_i(t)$ ($i = 1, 2, 3, 4$), $u(t)$, $Y(t)$, and $W(t)$ are bounded and $\theta(t)$ is positive and bounded.

3. Filter-Based Co-Estimation Method of SOH

Generally, the SOH of a new power battery is set to 100%, and with the use of the battery, the battery is aging and the SOH gradually decreases. When the capacity capability of a power battery decreases to 80% of its initial capacity, the battery is designated end of life (EOL) [4]. Therefore, the battery SOH is usually defined as follows:

$$SOH = \frac{C_0}{C_{0BOL}} \quad (8)$$

where C_0 is the current capacity of the battery and C_{0BOL} indicates the initial capacity of the battery. To identify the unknown parameter matrix in the battery model for the adaptive updating of the battery parameters and estimating the battery capacity to calculate the SOH, the unknown parameter matrix estimation error signal $\tilde{\theta} \in \mathbb{R}^8$ is defined as follows:

$$\tilde{\theta}(t) \triangleq \theta - \hat{\theta}(t) \quad (9)$$

where $\hat{\theta}(t) \in \mathbb{R}^8$ denotes the estimated value of the unknown parameter matrix. When designing the $\hat{\theta}(t)$ adaptive update rate for estimating the unknown parameter matrix using the least squares approach, we encounter the product term of the measurable variable matrix Y and the non-measurable variable matrix W . To address this challenge, we reference the design of filters in [33] and introduce a measurable filter $Y_f(t) \in \mathbb{R}^{1 \times 8}$ and a non-measurable filter $\eta(t) \in \mathbb{R}$, which are designed as follows:

$$\begin{cases} \dot{Y}_f = -\beta_4 Y_f + Y \hat{W} \\ \dot{\eta} = -\beta_4 \eta + Y \tilde{W} \theta \end{cases} \quad (10)$$

where $\beta_4 \in \mathbb{R}$ is the positive gain, and $Y \hat{W}$ and $Y \tilde{W} \theta$ denote the intermediate variables of the filtered signal. Refer to the algorithm designed in [34], the filter-based observer for the SOH estimation is designed as:

$$\begin{cases} \dot{\hat{x}}_1 = -a \hat{x}_1 - bu + \beta_1 \tilde{x}_4 \\ \dot{\hat{x}}_2 = -\hat{\theta}_1 \hat{x}_2 + \hat{\theta}_5 u + \beta_2 \tilde{x}_4 \\ \dot{\hat{x}}_3 = -\hat{\theta}_2 \hat{x}_3 + \hat{\theta}_6 u + \beta_3 \tilde{x}_4 \\ \dot{\hat{x}}_4 = Y \hat{W} \hat{\theta} + Y_f \dot{\hat{\theta}} + \beta_4 \tilde{x}_4 \end{cases} \quad (11)$$

where $\hat{x} \triangleq [\hat{x}_1 \ \hat{x}_2 \ \hat{x}_3 \ \hat{x}_4]^T \in \mathbb{R}^4$ is the state estimate, $\tilde{x}_i \triangleq x_i - \hat{x}_i$ ($i = 1, 2, 3, 4$) $\in \mathbb{R}$ denotes the state estimation error, and β_i ($i = 1, 2, 3, 4$) $\in \mathbb{R}$ represents the designed observer gain.

Based on Equations (7) and (11), the state estimation error is obtained as:

$$\begin{cases} \dot{\tilde{x}}_1 = -a \tilde{x}_1 - \beta_1 \tilde{x}_4 \\ \dot{\tilde{x}}_2 = h_1(x_2) - \hat{\theta}_1 \tilde{x}_2 - \beta_2 \tilde{x}_4 \\ \dot{\tilde{x}}_3 = h_2(x_3) - \hat{\theta}_2 \tilde{x}_3 - \beta_3 \tilde{x}_4 \\ \dot{\tilde{x}}_4 = Y W \theta - Y \hat{W} \hat{\theta} - Y_f \dot{\hat{\theta}} - \beta_4 \tilde{x}_4 \end{cases} \quad (12)$$

where $h_1 \triangleq -\tilde{\theta}_1 x_2 + \tilde{\theta}_5 u$ and $h_2 \triangleq -\tilde{\theta}_2 x_3 + \tilde{\theta}_6 u$ are bounded functions. The adaptive estimation update law for the unknown parameter matrix is designed as:

$$\dot{\hat{\theta}} \triangleq LY_f^T \tilde{x}_4 \quad (13)$$

where L is the parameter adaptive estimation gain and the recursive computation satisfies:

$$\frac{d}{dt} (L^{-1}) = Y_f^T Y_f. \quad (14)$$

In the subsequent analysis, $L^{-1}(0)$ is required to be positive definite. This requirement can be met by selecting an appropriate non-zero initial value.

Assumption 1. According to the analysis of Assumption 1 in [34], there are known constants M_1 and $M_2 \in \mathbb{R}_{>0}$, such that the functions $h_1(\cdot), h_2(\cdot)$ have upper bounds and satisfy $|h_1(\cdot)| \leq M_1$, $|h_2(\cdot)| \leq M_2$. Since the parameters of the battery model are all positive, there are constants d_1 and d_2 greater than 0, such that $|\hat{\theta}_1| \geq d_1$, $|\hat{\theta}_3| \geq d_2$.

The simultaneous addition of an $\tilde{W}\theta$ to Equation (12) can be rewritten as follows:

$$\dot{\tilde{x}}_4 = Y\tilde{W}\theta + Y\tilde{W}\tilde{\theta} - Y_f\dot{\hat{\theta}} - \beta_4\tilde{x}_4. \quad (15)$$

Combining Equations (10) and (15), the state error of x_4 can be expressed as:

$$\tilde{x}_4 = Y_f\tilde{\theta} + \eta + \mu e^{-\beta_4 t} \quad (16)$$

where $\mu \triangleq \tilde{x}_4(0) - Y_f(0)\tilde{\theta}(0) - \eta(0) \in \mathbb{R}$ is an unknown constant based on the initial conditions.

The flow chart of the estimation algorithm for the SOH of lithium-ion batteries based on filters is shown in Figure 2.

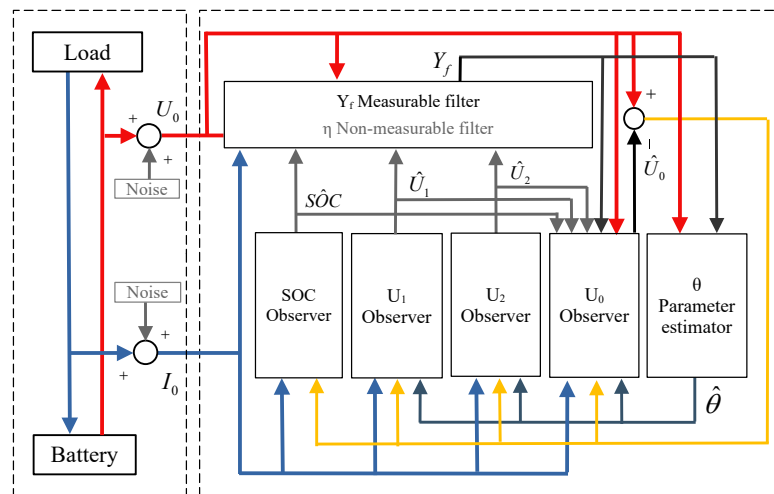


Figure 2. Flow chart of the estimation algorithm for SOH.

4. Stability Analysis

The stability of the nonlinear observer for the estimation of the SOH of lithium-ion batteries is analyzed according to the following theorem.

Theorem 1. For a nonlinear observer in Equation (11) using the parameter update rates defined in Equation (13), consider the equivalent model of the battery in Equation (7) and satisfy As-

sumption 1 to ensure that the state errors are consistently and ultimately bounded, and the gain condition satisfies:

$$\beta_4 > m + \frac{\gamma\beta_1^2}{2a_1} + \frac{3\beta_2^2}{4d_1} + \frac{3\beta_3^2}{4d_2} - Y_f L Y_f^T \quad (17)$$

with

$$k_1 > 4, k_2 > 2, k_3 > 4,$$

$$m > \frac{k_1 + \frac{1}{k_2} + (k_4 + k_7)\|Y\|_\infty^2}{1 - \frac{2}{k_2}} + \frac{\frac{1}{k_1} + (k_6 + k_9)\|Y\|_\infty^2}{1 - \frac{2}{k_3} - \frac{2}{k_1}} + k_2 + k_3 + (k_5 + k_8)\|Y\|_\infty^2.$$

To demonstrate the convergence of the designed nonlinear observer, a Lyapunov function $V(t) \in \mathbb{R}$ is chosen as follows:

$$V \triangleq \frac{1}{2}\alpha\tilde{x}_1^2 + \frac{1}{2}\tilde{x}_2^2 + \frac{1}{2}\tilde{x}_3^2 + \frac{1}{2}\tilde{x}_4^2 + \frac{1}{2}\eta^2 + \frac{1}{2}\tilde{\theta}^T L^{-1}\tilde{\theta} \quad (18)$$

where α is a positive constant, and L^{-1} is the inverse matrix of L and is positive definite. For subsequent calculations, the two nonlinear functions V_1 and V_2 are denoted as:

$$V_1 = \frac{1}{2}\alpha\tilde{x}_1^2 + \frac{1}{2}\tilde{x}_2^2 + \frac{1}{2}\tilde{x}_3^2 \quad (19)$$

$$V_2 = \frac{1}{2}\tilde{x}_4^2 + \frac{1}{2}\eta^2 + \frac{1}{2}\tilde{\theta}^T L^{-1}\tilde{\theta}. \quad (20)$$

According to the stability analysis of [34] and Assumption 1, it can be obtained:

$$\dot{V}_1 \leq -\frac{\alpha a}{2}\tilde{x}_1^2 - \frac{d_1}{3}\tilde{x}_2^2 - \frac{d_2}{3}\tilde{x}_3^2 + \left(\frac{\alpha\beta_1^2}{2a_1} + \frac{3\beta_2^2}{4d_1} + \frac{3\beta_3^2}{4d_2}\right)\tilde{x}_4^2 + \frac{3M_1^2}{4d_1} + \frac{3M_2^2}{4d_2}. \quad (21)$$

And, the time derivative of V_2 yields:

$$\begin{aligned} \dot{V}_2 &\leq -\left[m + 1 - k_1 - \frac{2m+1}{k_2} - (k_4 + k_7)\|Y\|_\infty^2\right]\|Y_f\tilde{\theta}\|^2 \\ &\quad - \left[\beta_4 + m - k_2 - k_3 - (k_5 + k_8)\|Y\|_\infty^2\right]\|\eta\|^2 \\ &\quad - \left[m - \frac{2m+1}{k_1} - \frac{2m}{k_3} - (k_6 + k_9)\|Y\|_\infty^2\right]\mu^2 e^{-2\beta_4 t} \\ &\quad + \left(\frac{1}{k_4} + \frac{1}{k_5} + \frac{1}{k_6}\right)(\|\tilde{W}\|_\infty\|\theta\|)^2 + \left(\frac{1}{k_7} + \frac{1}{k_8} + \frac{1}{k_9}\right)(\|\hat{W}\|_\infty\|\tilde{\theta}\|)^2 \end{aligned} \quad (22)$$

where $m < \beta_4 + Y_f L Y_f^T$ is a positive constant and $k_i(i = 1, 2, \dots, 9) \in \mathbb{R}$ is the positive constant described by the gain condition in Theorem 1.

According to Remark 1, the parameter estimates and the filter definition show that $W(t)$, $\tilde{W}(t)$, $\theta(t)$, and $\tilde{\theta}(t) \in \mathcal{L}_\infty$, which yields $(\|\tilde{W}\|_\infty\|\theta\|)^2$ and $(\|\hat{W}\|_\infty\|\tilde{\theta}\|)^2 \in \mathcal{L}_\infty$. Therefore, the last two terms of the above equation can be considered to have upper bounds. Finally, combining Equations (21) and (22) yields:

$$\dot{V}_1 \leq -\frac{\alpha a}{2}\tilde{x}_1^2 - \frac{d_1}{3}\tilde{x}_2^2 - \frac{d_2}{3}\tilde{x}_3^2 - \gamma\tilde{x}_4^2 - \lambda_1\|Y_f\tilde{\theta}\|^2 - \lambda_2\|\eta\|^2 - \lambda_3\mu^2 e^{-2\beta_4 t} + M \quad (23)$$

with

$$\lambda_1 = \left(1 - \frac{2}{k_2}\right)m + 1 - k_1 - \frac{1}{k_2} - (k_4 + k_7)\|Y\|_\infty^2,$$

$$\lambda_2 = \beta_4 + m - k_2 - k_3 - (k_5 + k_8)\|Y\|_\infty^2,$$

$$\begin{aligned}\lambda_3 &= \left(1 - \frac{2}{k_3} - \frac{2}{k_1}\right)m - \frac{1}{k_1} - (k_6 + k_9)\|Y\|_\infty^2, \\ \gamma &= \beta_4 + Y_f L Y_f^T - m - \frac{\alpha\beta_1^2}{2a_1} - \frac{3\beta_2^2}{4d_1} - \frac{3\beta_3^2}{4d_2}, \\ M &= \frac{3M_1^2}{4d_1} + \frac{3M_2^2}{4d_2} + \left(\frac{1}{k_4} + \frac{1}{k_5} + \frac{1}{k_6}\right)(\|\tilde{W}\|_\infty\|\theta\|)^2 + \left(\frac{1}{k_7} + \frac{1}{k_8} + \frac{1}{k_9}\right)(\|\hat{W}\|_\infty\|\tilde{\theta}\|)^2.\end{aligned}$$

Combining Assumption 1 shows that M is positively bounded. When γ and λ_i ($i = 1, 2, 3$) satisfy the gain condition in Theorem 1, for any $|\tilde{x}_1| > \sqrt{\frac{2M}{\alpha\alpha}}$, it follows that $\dot{V}_1 < 0$. Since the initial value of the Liapunov function $V_1(0) \in \mathcal{L}_\infty$, it follows that the state estimation error of the battery model is uniformly ultimately bounded. And, $|\tilde{x}_1| \leq \delta$, where δ satisfies $\sqrt{\frac{2M}{\alpha\alpha}} < \delta$.

5. Simulation Analysis and Experimental Results

5.1. Experimental Setup

To verify the estimation ability of the algorithm, an experimental platform was established to obtain the required data, as shown in Figure 3. The experimental platform consisted of a computer, a NEWARE CT-8008 battery testing system (NEWARE, Shenzhen, China), a RIUKAI R-TH-50 LKF programmable constant temperature and humidity test chamber (RIUKAI, Guangdong, China), and lithium-ion batteries. The control computer was equipped with a BTS 8.0.0 upper computer system, which can control the BTS to charge and discharge the battery in real time and record the battery data. The temperature test chamber ensured that the battery ambient temperature was within the set range. The model number of lithium-ion batteries used in experiments was INR18650 MH1, and the basic specifications of batteries are shown in Table 1.

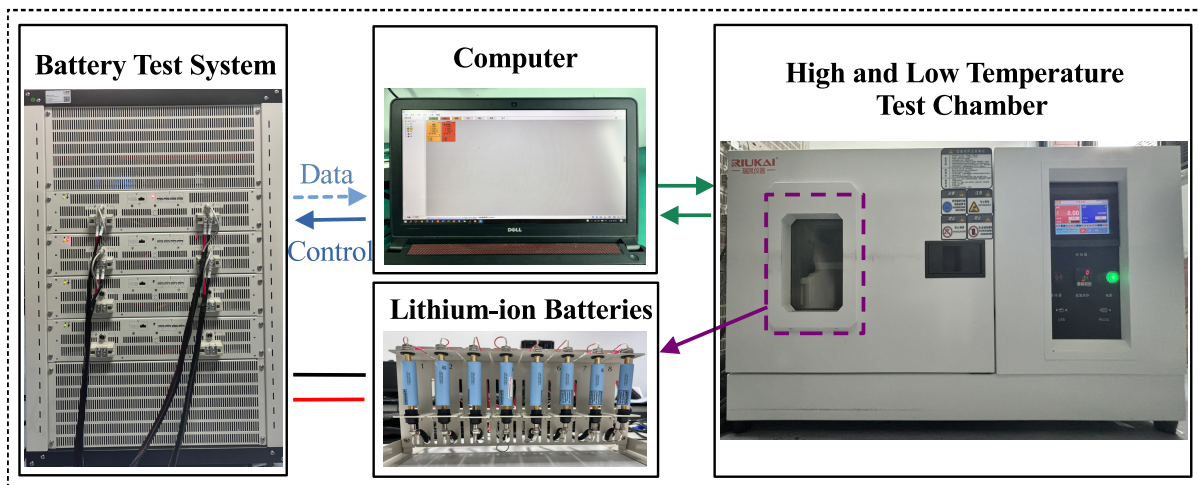


Figure 3. Experimental platform.

Table 1. Basic specifications of lithium–ion batteries.

Parameters	Specification
Rated capacity	3200 mAh
Nominal voltage	3.63 V
Maximum charge voltage	4.2 V
Discharge cut-off voltage	2.5 V
Working temperature	0~45 °C
Battery weight	49 g

Dynamic stress testing (DST) [39] and the Federal City Driving Schedule (FUDS) [40] were used to evaluate the battery algorithm performance. The former was primarily used to test the battery's charge and discharge power capabilities, which helped to verify the adaptability of battery model parameters under variable current conditions. The latter, based on actual vehicle driving patterns, speeds, accelerations, and other parameters in urban environments, aims to provide a testing condition that is closer to real-world usage scenarios, enabling the assessment of battery performance under actual urban driving conditions. Figure 4 demonstrates the current and voltage profiles of the DST and FUDS tests at 25 °C.

Basic performance tests under dynamic operating conditions were conducted on four groups of battery samples at 0 °C, 10 °C, 25 °C, and 45 °C. Each group contained two batteries for subsequent dynamic operating tests. The operating temperature was adjusted to 25 °C, and the battery underwent a capacity test and a rapid test procedure for identifying model parameters to obtain the initial battery parameters. The battery was then charged and discharged under DST and FUDS conditions until its SOC reached 0. The batteries were fully charged again, and the operating temperature was adjusted to 0 °C, 10 °C, and 45 °C, repeating the aforementioned experimental steps. The battery testing procedure is illustrated in Figure 5.

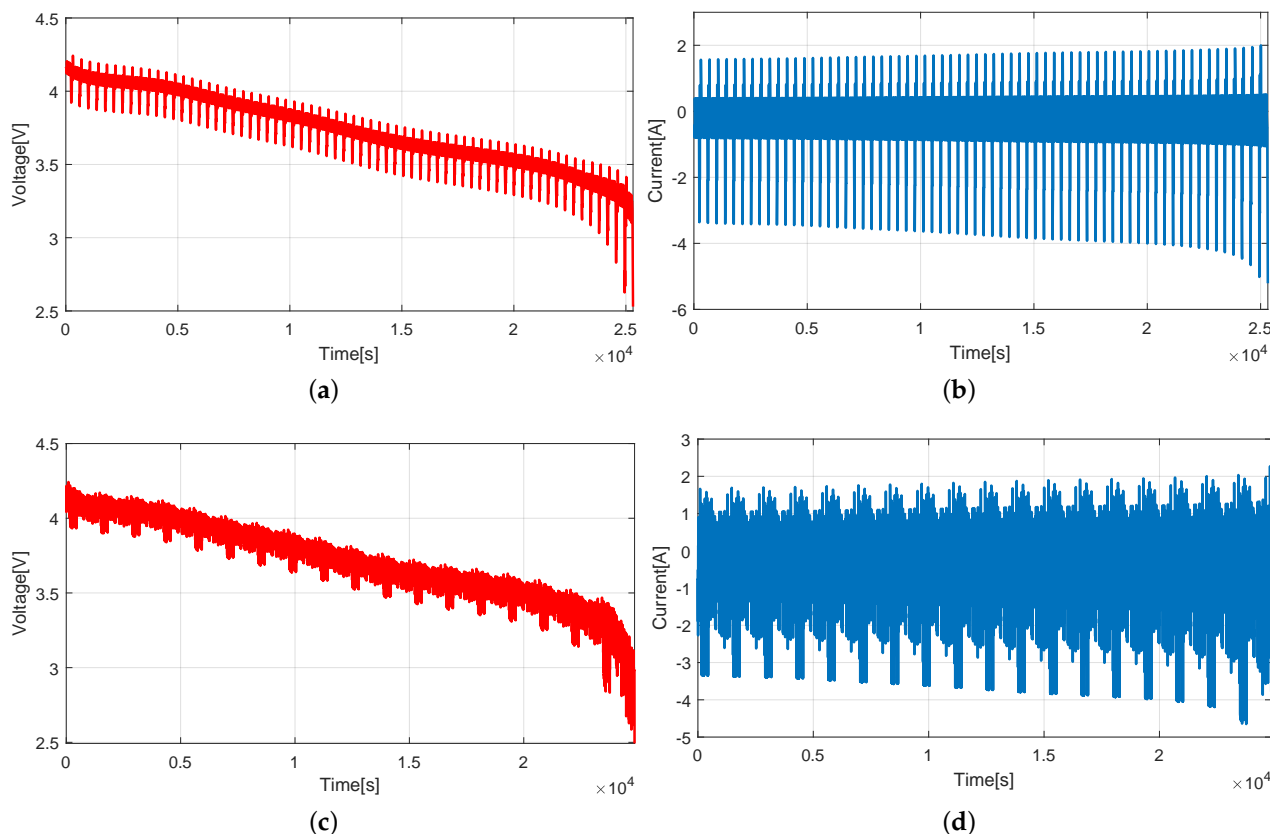


Figure 4. The current and voltage of DST and FUDS tests at 25 °C. (a) Terminal voltage under the DST condition; (b) current under the DST condition; (c) terminal voltage under the FUDS condition; (d) current under the FUDS condition.

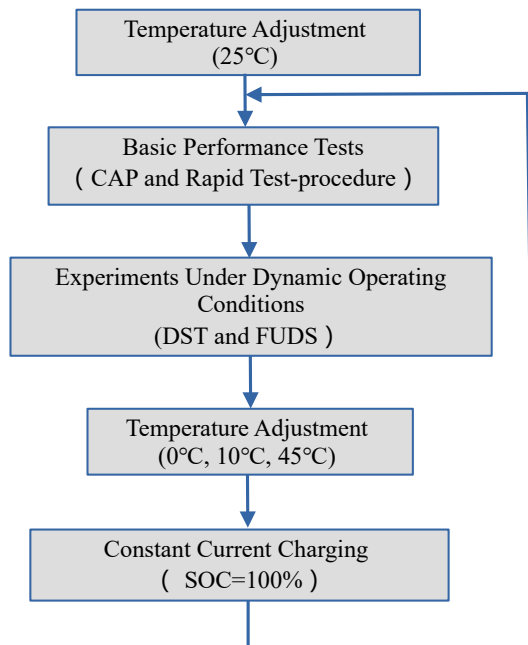


Figure 5. Flow chart of battery test procedure.

5.2. Lithium-Ion Battery Basic Performance Test

In order to obtain the relationship between the open-circuit voltage U_{OC} and the SOC of lithium-ion batteries at different temperatures, the experiments refer to the rapid test method in [16]. Firstly, the lithium-ion battery was charged to a SOC of 100%. The lithium-ion battery was then discharged to 10% of the rated capacity with a constant current of rated current (0.2 C), left to stand for 20 min, and then the above discharging operation was repeated until the SOC was 0. The battery current curve is shown in Figure 6.

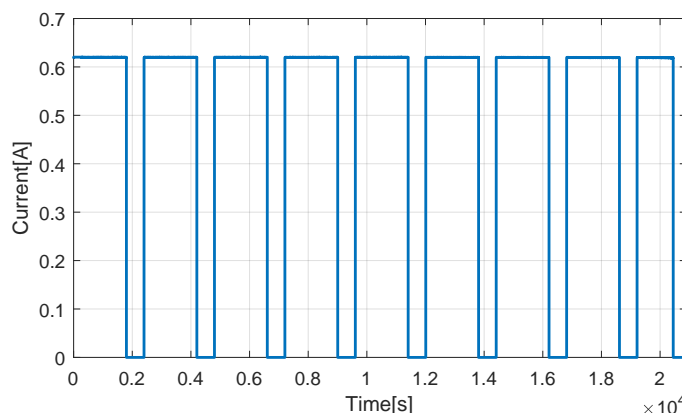


Figure 6. The current of rapid test procedure.

The open-circuit voltage U_{OC} corresponding to different SOCs was obtained experimentally, and an OCV model consisting of an exponential function and a polynomial was used to fit the function between the open-circuit voltage and the SOC of the battery. The chosen fitting model is as follows:

$$OCV = K_1 SOC + K_2 SOC^2 + K_3 SOC^3 + K_4 SOC^4 + K_5 SOC^5 + K_6 SOC^6.$$

The relationship curve between the SOC and V_{OC} at different temperatures is shown in Figure 7. The internal resistance of the second-order hybrid equivalent circuit model of the lithium-ion battery could be obtained by calculating the ratio of the transient voltage drop to the current; Moreover, the capacitance and resistance, which represent the long-term and short-term transient responses, could be obtained by utilizing the voltage-current response

curve fitting. The initial values of the battery model parameters at different temperatures are shown in Table 2.

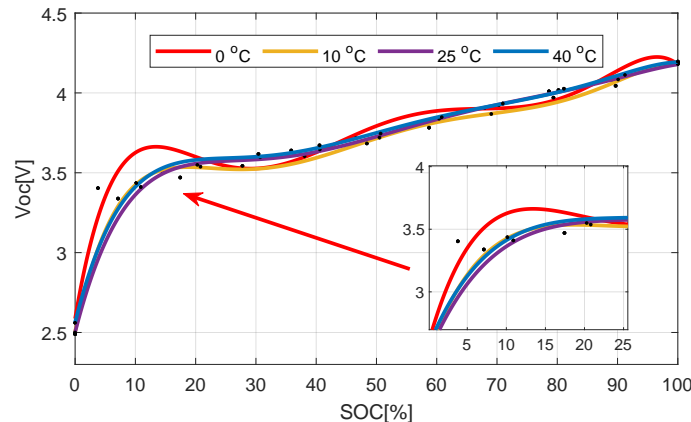


Figure 7. The open circuit voltage versus SOC of the battery at different temperatures.

Table 2. The initial values of the battery model parameters at different temperatures.

Temperature	R_0 (Ω)	R_s (Ω)	R_f (Ω)	C_0 (F)	C_s (F)	C_f (F)
0 °C	0.053	0.022	0.034	2.764	46.429	9263.228
10 °C	0.042	0.099	0.043	2.970	5.482	2747.428
25 °C	0.029	0.056	0.054	3.047	12.443	2462.632
40 °C	0.013	0.077	0.041	3.179	6.99	3905.739

5.3. Experiment under Dynamic Operating Conditions

In order to highlight the estimation superiority of the developed algorithm, the proposed method was tested under DST and FUDS conditions, and the DEKF [27,41] and DUKF [29,42] methods were introduced to compare the results under 25 °C. Assuming that the initial SOC value was 0.9, the real SOC value, the estimation results using this method, the estimation results with the DEKF and DUKF methods, and the corresponding errors are shown in Figure 8. The real reference value of SOC was obtained by the CCM. The DUKF method is capable of resolving the potential issues of the DEKF in highly nonlinear systems. However, while the DUKF method exhibited improved algorithmic performance compared to the DEKF, it still failed to take into account all parameters of the battery model. On the other hand, the filter-based observer estimated the battery model parameters, enhancing modeling accuracy. It can be seen from Figure 8 that, compared with the DEKF and DUKF, the filter-based observer had a better estimation accuracy and faster dynamic response speed.

The SOH value was determined by substituting the estimated capacity C_0 and the initial capacity C_{0BOL} into Equation (8), and the reference value of the true SOH value was obtained by fitting the capacity obtained from the capacity test before and after the cycle. Figure 9 shows the true value of the SOH, the estimation results of the SOH using this method, and the estimation results of the DEKF and DUKF. It can be seen that the filter-based observer had a better applicability than the DEKF for different working conditions and had a better estimation accuracy.

Tests based on DST and FUDS conditions at 0 °C, 10 °C, and 45 °C were added to better verify the robustness of the algorithm at different temperatures. In order to analyze the superiority of the filter-based observer in estimation performance, it was compared with the DEKF and DUKF. The maximum absolute error (MAE) and the root mean square error (RMSE) were selected as evaluation indicators, and the estimated results at different temperatures are shown in Tables 3 and 4.

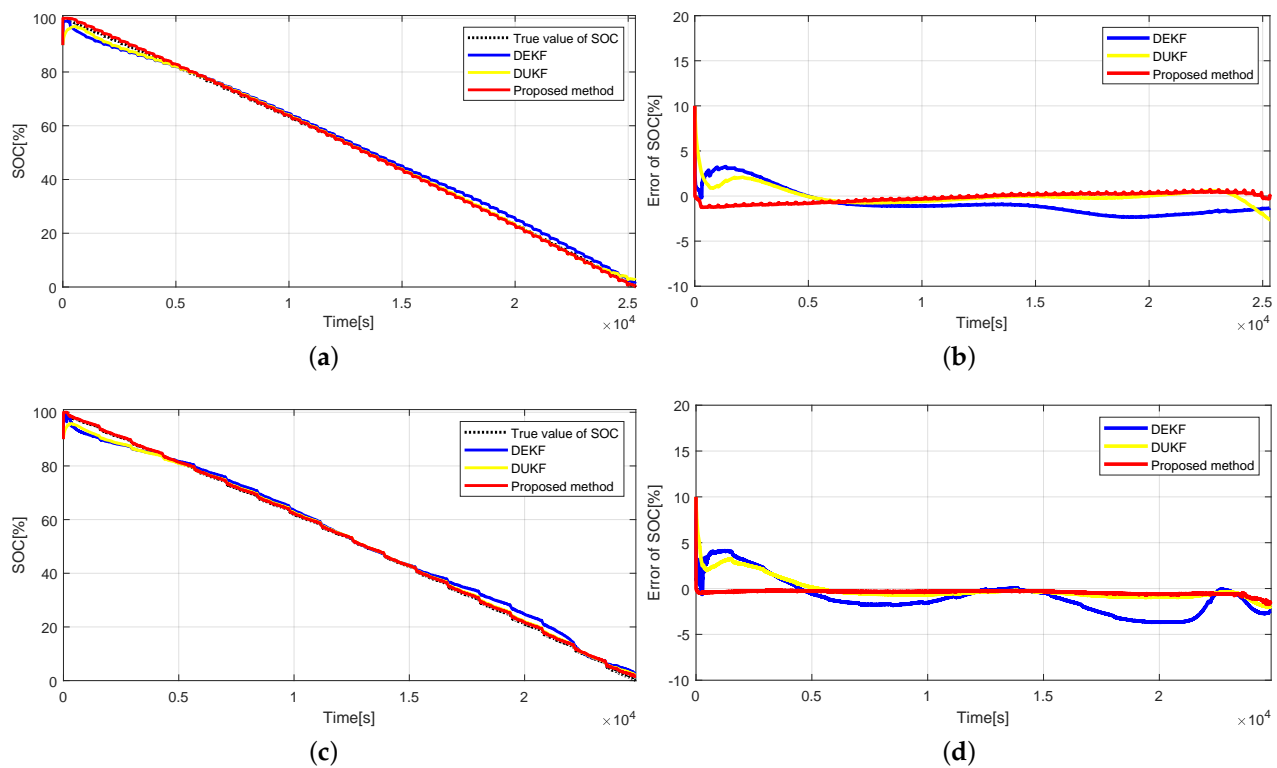


Figure 8. SOC estimation results under 25 °C. (a) Estimation results under the DST condition. (b) Estimation errors under the DST condition. (c) Estimation results under the FUDS condition. (d) Estimation errors under the FUDS condition.

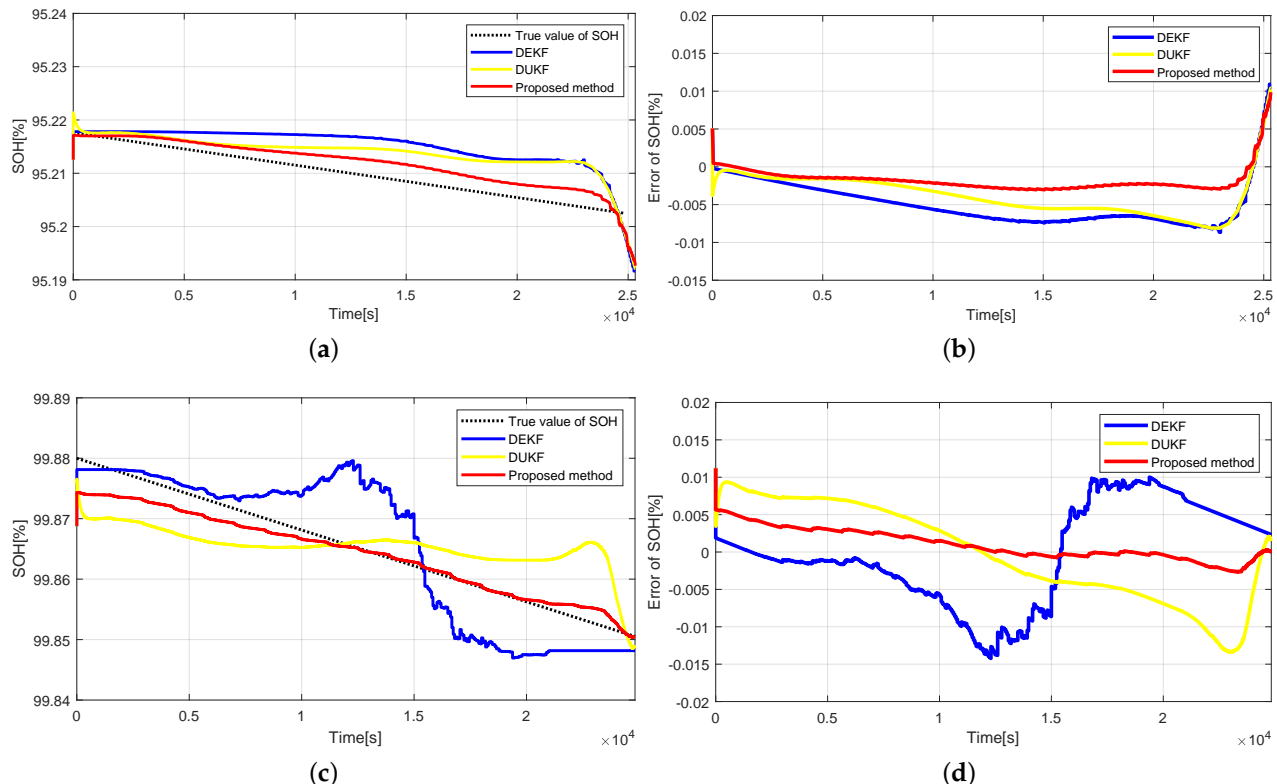


Figure 9. SOH estimation results under 25 °C. (a) Estimation results under the DST condition. (b) Estimation errors under the DST condition. (c) Estimation results under the FUDS condition. (d) Estimation errors under the FUDS condition.

Table 3. SOC estimation error results.

Temperature	Algorithm Type	DST Condition	FUDS Condition
0 °C	Filter-Based Observer	MAE: 1.1296%	MAE: 1.5110%
		RMSE: 0.5123%	RMSE: 0.8781%
		MAE: 9.0690%	MAE: 6.0277%
	DUKF	RMSE: 3.2567%	RMSE: 2.6664%
		MAE: 8.4087%	MAE: 6.1495%
		RMSE: 2.3025%	RMSE: 3.2103%
10 °C	Filter-Based Observer	MAE: 1.4766%	MAE: 1.0435%
		RMSE: 0.8685%	RMSE: 0.7620%
		MAE: 9.6849%	MAE: 9.5598%
	DUKF	RMSE: 4.0638%	RMSE: 3.9750%
		MAE: 9.1705%	MAE: 5.8272%
		RMSE: 5.3467%	RMSE: 3.6444%
25 °C	Filter-Based Observer	MAE: 1.2475%	MAE: 1.7281%
		RMSE: 0.5517%	RMSE: 0.4770%
		MAE: 3.2238%	MAE: 3.5548%
	DUKF	RMSE: 0.8014%	RMSE: 1.1321%
		MAE: 3.2698%	MAE: 4.1347%
		RMSE: 1.6472%	RMSE: 2.1402%
40 °C	Filter-Based Observer	MAE: 1.2621%	MAE: 0.3129%
		RMSE: 0.7205%	RMSE: 0.0975%
		MAE: 2.3814%	MAE: 3.4679%
	DUKF	RMSE: 0.9114%	RMSE: 0.9373%
		MAE: 2.9840%	MAE: 3.2516%
		RMSE: 1.8293%	RMSE: 0.7150%

Table 4. SOH estimation error results.

Temperature	Algorithm Type	DST Condition	FUDS Condition
0 °C	Filter-Based Observer	MAE: 0.0360%	MAE: 0.0112%
		RMSE: 0.0196%	RMSE: 0.0085%
		MAE: 0.0788%	MAE: 0.0478%
	DUKF	RMSE: 0.0372%	RMSE: 0.0246%
		MAE: 0.0732%	MAE: 0.0705%
		RMSE: 0.0278%	RMSE: 0.0325%
10 °C	Filter-Based Observer	MAE: 0.0239%	MAE: 0.0345%
		RMSE: 0.0183%	RMSE: 0.0054%
		MAE: 0.0292%	MAE: 0.0457%
	DUKF	RMSE: 0.0200%	RMSE: 0.0098%
		MAE: 0.0350%	MAE: 0.1429%
		RMSE: 0.0207%	RMSE: 0.0215%
25 °C	Filter-Based Observer	MAE: 0.0099%	MAE: 0.0078%
		RMSE: 0.0024%	RMSE: 0.0061%
		MAE: 0.0104%	MAE: 0.0186%
	DUKF	RMSE: 0.0046%	RMSE: 0.0089%
		MAE: 0.0109%	MAE: 0.0213%
		RMSE: 0.0057%	RMSE: 0.0103%
40 °C	Filter-Based Observer	MAE: 0.0383%	MAE: 0.0311%
		RMSE: 0.0116%	RMSE: 0.0168%
		MAE: 0.0227%	MAE: 0.0424%
	DUKF	RMSE: 0.0119%	RMSE: 0.0196%
		MAE: 0.0540%	MAE: 0.0499%
		RMSE: 0.0184%	RMSE: 0.0225%

For lithium-ion batteries, under low-temperature conditions, the internal resistance of the battery increases, the electrochemical reaction speed slows down, the internal resistance of polarization rapidly increases, and the capacity rapidly decreases. In the case of high temperatures, the battery capacity is not equal to that at room temperature, but due to the acceleration of the side reaction, the capacity attenuation is also accelerated. Tables 3 and 4 show that at 0 °C, 10 °C, 25 °C, and 45 °C, the filter-based observer performed well in the two error indexes of SOC and SOH estimation. The MAE and RMSE of the filter-based observer for SOC estimation were no more than 2% and 1%, and the MAE and RMSE for SOH estimation were no more than 0.5% and 0.2%.

At room temperature, the filter-based observer exhibited the best SOH estimation performance, with MAE and RMSE for SOH estimation not exceeding 0.1% and 0.1%. In high- and low-temperature environments, compared to the DEKF, the DUKF did not exhibit a significant advantage. This was due to the variations in battery model parameters caused by temperature changes, which affected the modeling accuracy. However, the filter-based method demonstrated superior estimation performance across different operating conditions under varying temperatures. It is evident that the accuracy of battery SOH estimation depends not only on algorithmic performance but also on the modeling accuracy of the battery model.

Although this paper uses fitting curves of SOC and V_{OC} at different temperatures to reduce the impact of temperature on the algorithm, the temperature during battery operation did not change linearly. The segmented selection mode of the SOC and V_{OC} fitting curves could not fully adapt to the effects of battery temperature changes. Therefore, the SOH estimation error increased at low and high temperatures, but the magnitude of the increase was significantly lower compared to the DEKF and DUKF methods, verifying that the filter-based algorithm exhibits good environmental adaptability at different temperatures. In the future, this method can be further optimized and improved. For instance, more advanced algorithms and technologies, such as machine learning and deep learning, can be introduced to enhance estimation accuracy and robustness.

6. Conclusions

In this paper, a filter-based method for estimating the SOH of lithium-ion batteries is proposed. First, the hybrid model of the battery was reconstructed to describe the terminal voltage derivatives in terms of the product of the measurable variable matrix, the non-measurable variable matrix, and the unknown parameter matrix. In order to obtain an adaptive battery model, the unknown parameter matrix was designed using an adaptive update rate utilizing signal filters. On this basis, a nonlinear observer with non-measurable variables is proposed to realize SOH estimation. Under conditions of 0 °C, 10 °C, 25 °C, and 45 °C, the MAE and RMSE of SOC estimation were less than 2% and 1%, while the MAE and RMSE of SOH estimation were less than 0.5% and 0.2%. The experimental results demonstrate that this method exhibits high estimation accuracy under various temperature conditions, providing a more efficient and accurate solution for electric vehicle battery management. Additionally, this method can be applied to more types of batteries and EVs to promote the continuous development of EVs technology.

Author Contributions: Conceptualization, X.W., J.C. and Y.L.; methodology, X.W. and J.C.; software, X.W.; validation, X.W., J.C. and Y.L.; formal analysis, X.W. and J.C.; investigation, X.W.; resources, J.C. and Y.L.; data curation, X.W. and H.T.; writing—original draft preparation, X.W.; writing—review and editing, X.W., J.C., H.T., K.X., M.S. and Y.L.; visualization, X.W.; supervision, X.W., J.C. and Y.L.; project administration, J.C. and Y.L.; funding acquisition, J.C. and Y.L. All authors have read and agreed to the published version of the manuscript.

Funding: This research has received funding from the Key Research and Development Program of Zhejiang Province under (Grant No. 2021C01098), the National Key R&D Program of China (No. 2022YFB4601601), and the Key R&D Program of Guangxi Province (Grant No. GKAB23026101).

Data Availability Statement: The data presented in this paper were used for the project of Wanxiang A123 Systems Corp. and are available on request from the corresponding author.

Conflicts of Interest: Authors Ke Xu and Mingding Shao were employed by the Department of System Engineering, Wanxiang A123 Systems Corp. The remaining authors declare that the research was conducted in the absence of any commercial or financial relationships that could be construed as a potential conflict of interest.

References

1. Yang, B.; Qian, Y.; Li, Q.; Chen, Q.; Wu, J.; Luo, E.; Xie, R.; Zheng, R.; Yan, Y.; Su, S.; et al. Critical summary and perspectives on state-of-health of lithium-ion battery. *Renew. Sustain. Energy Rev.* **2024**, *190*, 114077. [[CrossRef](#)]
2. Xiong, R.; Pan, Y.; Shen, W.; Li, H.; Sun, F. Lithium-ion battery aging mechanisms and diagnosis method for automotive applications: Recent advances and perspectives. *Renew. Sustain. Energy Rev.* **2020**, *131*, 110048. [[CrossRef](#)]
3. Liu, D.; Xie, W.; Liao, H.; Peng, Y. An integrated probabilistic approach to lithium-ion battery remaining useful life estimation. *IEEE Trans. Instrum. Meas.* **2014**, *64*, 660–670.
4. Dai, H.; Wei, X.; Sun, Z. A new SOH prediction concept for the power lithium-ion battery used on HEVs. In Proceedings of the 2009 IEEE Vehicle Power and Propulsion Conference, Dearborn, MI, USA, 7–10 September 2009; IEEE: Piscataway, NJ, USA, 2009; pp. 1649–1653.
5. Samadani, E.; Mastali, M.; Farhad, S.; Fraser, R.A.; Fowler, M. Li-ion battery performance and degradation in electric vehicles under different usage scenarios. *Int. J. Energy Res.* **2016**, *40*, 379–392. [[CrossRef](#)]
6. Pradhan, S.K.; Chakraborty, B. Battery management strategies: An essential review for battery state of health monitoring techniques. *J. Energy Storage* **2022**, *51*, 104427. [[CrossRef](#)]
7. Waag, W.; Käbitz, S.; Sauer, D.U. Experimental investigation of the lithium-ion battery impedance characteristic at various conditions and aging states and its influence on the application. *Appl. Energy* **2013**, *102*, 885–897. [[CrossRef](#)]
8. Choi, W.; Shin, H.C.; Kim, J.M.; Choi, J.Y.; Yoon, W.S. Modeling and applications of electrochemical impedance spectroscopy (EIS) for lithium-ion batteries. *J. Electrochem. Sci. Technol.* **2020**, *11*, 1–13. [[CrossRef](#)]
9. Han, X.; Ouyang, M.; Lu, L.; Li, J.; Zheng, Y.; Li, Z. A comparative study of commercial lithium ion battery cycle life in electrical vehicle: Aging mechanism identification. *J. Power Sources* **2014**, *251*, 38–54. [[CrossRef](#)]
10. Meng, K.; Chen, X.; Zhang, W.; Chang, W.; Xu, J. A robust ultrasonic characterization methodology for lithium-ion batteries on frequency-domain damping analysis. *J. Power Sources* **2022**, *547*, 232003. [[CrossRef](#)]
11. Schaltz, E.; Stroe, D.I.; Nørregaard, K.; Ingvardsen, L.S.; Christensen, A. Incremental capacity analysis applied on electric vehicles for battery state-of-health estimation. *IEEE Trans. Ind. Appl.* **2021**, *57*, 1810–1817. [[CrossRef](#)]
12. Zhang, S.; Guo, X.; Dou, X.; Zhang, X. A rapid online calculation method for state of health of lithium-ion battery based on coulomb counting method and differential voltage analysis. *J. Power Sources* **2020**, *479*, 228740. [[CrossRef](#)]
13. Xiong, R.; Li, L.; Tian, J. Towards a smarter battery management system: A critical review on battery state of health monitoring methods. *J. Energy Storage* **2018**, *405*, 18–29. [[CrossRef](#)]
14. Chen, Z.; Mi, C.C.; Fu, Y.; Xu, J.; Gong, X. Online battery state of health estimation based on Genetic Algorithm for electric and hybrid vehicle applications. *J. Power Sources* **2013**, *240*, 184–192. [[CrossRef](#)]
15. Ecker, M.; Gerschler, J.B.; Vogel, J.; Käbitz, S.; Hust, F.; Dechent, P.; Sauer, D.U. Development of a lifetime prediction model for lithium-ion batteries based on extended accelerated aging test data. *J. Power Sources* **2012**, *215*, 248–257. [[CrossRef](#)]
16. Jia, S.; Ma, B.; Guo, W.; Li, Z.S. A sample entropy based prognostics method for lithium-ion batteries using relevance vector machine. *J. Manuf. Syst.* **2021**, *61*, 773–781. [[CrossRef](#)]
17. Xiong, R.; Sun, Y.; Wang, C.; Tian, J.; Chen, X.; Li, H.; Zhang, Q. A data-driven method for extracting aging features to accurately predict the battery health. *Energy Storage Mater.* **2023**, *57*, 460–470. [[CrossRef](#)]
18. Manoharan, A.; Begam, K.; Aparow, V.R.; Sooriamoorthy, D. Artificial Neural Networks, Gradient Boosting and Support Vector Machines for electric vehicle battery state estimation: A review. *J. Energy Storage* **2022**, *55*, 105384. [[CrossRef](#)]
19. Zhao, J.; Han, X.; Ouyang, M.; Burke, A.F. Specialized deep neural networks for battery health prognostics: Opportunities and challenges. *J. Energy Chem.* **2023**, *87*, 416–438. [[CrossRef](#)]
20. Wu, L.; Lyu, Z.; Huang, Z.; Zhang, C.; Wei, C. Physics-based battery SOC estimation methods: Recent advances and future perspectives. *J. Energy Chem.* **2023**, *89*, 27–40. [[CrossRef](#)]
21. Vaghela, R.; Ramani, P.; Sarda, J.; Hui, K.L.; Sain, M. Analysis of State-of-Health Estimation Approaches and Constraints for Lithium-Ion Batteries in Electric Vehicles. *Int. J. Energy Res.* **2024**, *2024*, 6488186. [[CrossRef](#)]
22. Sarkar, S.; Halim, S.Z.; El-Halwagi, M.M.; Khan, F.I. Electrochemical models: Methods and applications for safer lithium-ion battery operation. *J. Electrochem. Soc.* **2022**, *169*, 100501. [[CrossRef](#)]
23. Naseri, F.; Schaltz, E.; Stroe, D.I.; Gismero, A.; Farjah, E. An enhanced equivalent circuit model with real-time parameter identification for battery state-of-charge estimation. *IEEE Trans. Ind. Electron.* **2021**, *69*, 3743–3751. [[CrossRef](#)]
24. Zhou, Z.; Zhang, C. An Extended Kalman Filter Design for State-of-Charge Estimation Based on Variational Approach. *Batteries* **2023**, *9*, 583. [[CrossRef](#)]

25. Tian, Y.; Xia, B.; Sun, W.; Xu, Z.; Zheng, W. A modified model based state of charge estimation of power lithium-ion batteries using unscented Kalman filter. *J. Power Sources* **2014**, *270*, 619–626. [[CrossRef](#)]
26. Schwunk, S.; Armbruster, N.; Straub, S.; Kehl, J.; Vetter, M. Particle filter for state of charge and state of health estimation for lithium–iron phosphate batteries. *J. Power Sources* **2013**, *239*, 705–710. [[CrossRef](#)]
27. Plett, G.L. Extended Kalman filtering for battery management systems of LiPB-based HEV battery packs: Part 3. State and parameter estimation. *J. Power Sources* **2004**, *134*, 277–292. [[CrossRef](#)]
28. Xiong, R.; Sun, F.; Chen, Z.; He, H. A data-driven multi-scale extended Kalman filtering based parameter and state estimation approach of lithium-ion polymer battery in electric vehicles. *Appl. Energy* **2014**, *113*, 463–476. [[CrossRef](#)]
29. Xiong, R.; Mu, H. Accurate state of charge estimation for lithium-ion battery using dual Unscented Kalman filters. In Proceedings of the 2017 Chinese Automation Congress (CAC), Jinan, China, 20–22 October 2017; IEEE: Piscataway, NJ, USA, 2017; pp. 5484–5487.
30. Yu, Q.; Xiong, R.; Yang, R.; Pecht, M.G. Online capacity estimation for lithium-ion batteries through joint estimation method. *Appl. Energy* **2019**, *255*, 113817. [[CrossRef](#)]
31. Lai, X.; Yuan, M.; Tang, X.; Yao, Y.; Weng, J.; Gao, F.; Ma, W.; Zheng, Y. Co-estimation of state-of-charge and state-of-health for lithium-ion batteries considering temperature and ageing. *Energies* **2022**, *15*, 7416. [[CrossRef](#)]
32. Zhou, M.; Wei, K.; Wu, X.; Weng, L.; Su, H.; Wang, D.; Zhang, Y.; Li, J. Fractional-Order Sliding-Mode Observers for the Estimation of State-of-Charge and State-of-Health of Lithium Batteries. *Batteries* **2023**, *9*, 213. [[CrossRef](#)]
33. Chen, J.; Chitrakaran, V.K.; Dawson, D.M. Range identification of features on an object using a single camera. *Automatica* **2011**, *47*, 201–206. [[CrossRef](#)]
34. Wu, X.; Chen, J.; Wang, D.; Xu, K.; Shao, M.; Wang, Y.; Long, Y. Filter-Based Co-estimation of State-of-Charge and State-of-Health for Lithium-ion Batterie. *IEEE Trans. Ind. Electron.* **2024**, submitted.
35. Chen, M.; Rincon-Mora, G.A. Accurate electrical battery model capable of predicting runtime and IV performance. *IEEE Trans. Energy Convers.* **2006**, *21*, 504–511. [[CrossRef](#)]
36. Chen, J.; Ouyang, Q.; Xu, C.; Su, H. Neural network-based state of charge observer design for lithium-ion batteries. *IEEE Trans. Control Syst. Technol.* **2018**, *26*, 313–320. [[CrossRef](#)]
37. Chaoui, H.; Mandalapu, S. Comparative study of online open circuit voltage estimation techniques for state of charge estimation of lithium-ion batteries. *Batteries* **2017**, *3*, 12. [[CrossRef](#)]
38. Rahman, M.A.; Anwar, S.; Izadian, A. Electrochemical model parameter identification of a lithium-ion battery using particle swarm optimization method. *J. Power Sources* **2016**, *307*, 86–97. [[CrossRef](#)]
39. Wang, Y.; Liu, C.; Pan, R.; Chen, Z. Experimental data of lithium-ion battery and ultracapacitor under DST and UDDS profiles at room temperature. *Data Brief* **2017**, *12*, 161–163. [[CrossRef](#)] [[PubMed](#)]
40. He, H.; Xiong, R.; Fan, J. Evaluation of lithium-ion battery equivalent circuit models for state of charge estimation by an experimental approach. *Energies* **2011**, *4*, 582–598. [[CrossRef](#)]
41. Yang, F.; Xu, Y.; Su, L.; Yang, Z.; Feng, Y.; Zhang, C.; Shao, T. State of charge and state of health estimation of lithium-ion battery packs with inconsistent internal parameters using dual extended Kalman filter. *J. Electrochim. Energy Convers. Storage* **2024**, *21*, 011004. [[CrossRef](#)]
42. Mahboubi, D.; Gavzani, I.J.; Saidi, M.H.; Ahmadi, N. State of charge estimation for lithium-ion batteries based on square root sigma point Kalman filter considering temperature variations. *IET Electr. Syst. Transp.* **2022**, *12*, 165–180. [[CrossRef](#)]

Disclaimer/Publisher’s Note: The statements, opinions and data contained in all publications are solely those of the individual author(s) and contributor(s) and not of MDPI and/or the editor(s). MDPI and/or the editor(s) disclaim responsibility for any injury to people or property resulting from any ideas, methods, instructions or products referred to in the content.